

# Symmetry breaking in the free surface of rotating fluids with high Reynolds numbers



## A Bachelor Project by

Thomas R. N. Jansson    Martin P. Haspang    Kåre H. Jensen  
tjansson@fys.ku.dk    haalle@fys.ku.dk    hartvig@fys.ku.dk  
191182-xxxx    270480-xxxx    020780-xxxx

## Supervised by

Professor Tomas Bohr  
Department of Physics  
Technical University of Denmark

University of Copenhagen, December 2004

The authors contributed with 1/3 each.

Pictures, movies and the project can be found at at:

<http://www.fys.ku.dk/~tjansson/bachelor.html>

## Abstract

The flow of water on a rotating plate in an open non rotating cylinder is studied. Strong symmetry breaking where the free surface forms in a non axis symmetric way is observed. The system is operated at high Reynolds numbers ( $10^5 - 10^6$ ) and the character of the symmetry breaking is studied by varying  $H$ ,  $\omega$  and  $\nu$ . It turns out that the number of corners in the observed shapes increases with frequency, and decreases when the water level is increased. Changing viscosity does surprisingly not lead to big changes in the phase diagram and thus the Reynolds number does not necessarily describe the system well. We investigate the effect of perturbing the system with various mechanical disturbances and the effect of changing the surface tension. For large ranges of frequencies, the shapes are stable to mechanical perturbations, while it is seen that they become unstable close to the transition between two shapes. It is also found that forced misalignments of cylinder and bottom plate have no observable influence on the shapes, so we believe we are dealing with spontaneous symmetry breaking. However, we found that changing the surface tension introduces some change in the phase diagram. Much has been written about the subject of the flow of a fluid in open cylinder with a rotating bottom plate but none of literature encountered has reported the spectacular deformations in the free surface observed in this experiment.

---

Thomas R. N. Jansson    Martin P. Haspang    Kåre H. Jensen

## Acknowledgments

The authors wish to thank our supervisor Tomas Bohr and Pascal Hersen who has been an invaluable source of advice throughout the process of making this project.

# Contents

|   |           |
|---|-----------|
| <b>Introduction</b>   | <b>1</b>  |
| 1.1 Flow characteristics . . . . .                                    | 3         |
| 1.1.1 The Reynolds number . . . . .                                   | 3         |
| 1.1.2 The Froude number . . . . .                                     | 4         |
| 1.2 Fluids in rotation . . . . .                                      | 4         |
| 1.2.1 A simple model: Fluids in almost solid body rotation . . . . .  | 4         |
| <b>Setup and methods</b>  | <b>8</b>  |
| 2.1 Technical description . . . . .                                   | 8         |
| 2.2 Measurements . . . . .  | 9         |
| 2.3 Experimental method and observations . . . . .                    | 11        |
| <b>Results</b>  | <b>13</b> |
| 3.1 Phase diagram . . . . .   | 13        |
| 3.1.1 Water in 131mm container . . . . .                              | 13        |
| 3.1.2 Water in 194mm container . . . . .                              | 15        |
| 3.2 Phase locking . . . . .   | 16        |
| 3.3 Hysteresis . . . . .  | 16        |
| 3.4 The effect of changing key parameters in the experiment . . . . . | 17        |
| 3.4.1 Substituting water with Ethylene Glycol . . . . .               | 17        |
| 3.4.2 Changing the surface tension . . . . .                          | 18        |
| 3.4.3 Misaligning the cylinder . . . . .                              | 18        |
| 3.5 Stability and time evolution of the states . . . . .              | 18        |
| <b>Discussion</b>   | <b>24</b> |
| 4.1 Discussion of the results . . . . .                               | 24        |
| 4.1.1 Phase diagram . . . . .   | 24        |
| 4.1.2 Symmetry breaking, viscosity, and the Reynolds number . . . . . | 24        |
| 4.1.3 Aspect ratio and the water level . . . . .                      | 26        |
| 4.1.4 Transitions between different states . . . . .                  | 26        |
| 4.1.5 Rotating vortices . . . . .                                     | 27        |
| 4.2 Other work of interest . . . . .                                  | 27        |
| 4.2.1 Other experiments concerning cylindrical flows . . . . .        | 27        |
| 4.2.2 Similar symmetry breaking in other systems . . . . .            | 28        |
| 4.3 Future work . . . . .   | 29        |
| 4.4 Concluding remarks . . . . .                                      | 30        |
| <b>Notation</b>   | <b>31</b> |
| <b>Bibliography</b>   | <b>32</b> |
| <b>Appendix</b>   | <b>33</b> |
| A.1 The von Kármán model . . . . .                                    | 33        |

# Introduction

A simple experiment can be made where water in a cylinder is rotated by the bottom plate and the surface is free. When this experiment is made, it is expected that the surface deforms as a circular shape when seen from above, e.g. as seen in Newton's bucket<sup>1</sup>.

We conducted the experiment and something surprising happened when we started to change the rotational rate of the bottom plate. The expected round shape of the surface of the water changed dramatically for some certain rotational rates. Instead of the usual round shape we discovered the formation of elliptic, triangular, quadratic etc. shapes in the free surface of the water when varying the rotational rate and the depth of the water. The deformations of the surface are so large that they are easily seen by the human eye. When the rotational rate of the plate is great enough, the deformation of the surface is seen to persist all the way down to the plate, which makes the phenomenon even more spectacular (see figure 1.1).

Even though we have used a lot of effort on searching the literature for similar observations we have found nothing directly comparable to the experiment we have made. This comes as a bit of a surprise to us, since similar systems has been studied a lot.

Much effort has previously been put into understanding the flow produced above a rotating disk in a fixed cylindrical container with an open top. These experiments are usually operated at so low rotational rates that the free surface of the water has remained essentially flat and horizontal. Most of the effort has been put into understanding the internal flows. Symmetry breaking in these internal flows has also been studied in detail. Some of the patterns that have been observed in these flows exhibit a structure with a kind of corners that look a bit like the ones we have seen. However, these patterns are not seen as deformations in the free surface and it seems that they are of a different character than the shapes we observe.

In this project we will investigate these shapes, their characteristics and try to give a possible explanation as to why they occur. The flows in the cylinder are very complicated to calculate since the free surface and it's shape should be taken into account. Calculating these flows reaches beyond the limitations of the project.

The project is experimental and centered around observations of the phenomena and the interpretation of these. We will introduce a phase diagram for each of the two setups and try to perturbate the system in many ways to reveal it's characteristics. The natural question as to why the phenomenon occur is difficult to answer due to the very complicated flow of the water, but we will make an attempt to make a qualified guess based on the literature and observations.

Trying to understand the fundamental dynamics of the system, we will start off with a presentation of the parameters that determine the flow characteristics followed by a description of fluids in rotation.

---

<sup>1</sup>Newton's bucket is a rotating cylinder where both the bottom and walls are rotating. Eventually the surface will be perpendicular to the fictive gravity field.



(a)  $k = 0$



(b)  $k = 2$



(c)  $k = 3$



(d)  $k = 4$



(e)  $k = 5$



(f)  $k = 6$

Figure 1.1: *The different kinds of shapes that appear in the free surface for the 131 mm setup.  $k$  denotes the number of corners in the shapes. Only shapes that reach the bottom plate are shown, since they are easier to photograph. Far most of the shapes we observe are symmetric like the ones shown here, but more irregular shapes have also been observed.*

## 1.1 Flow characteristics

The general behavior of fluids in motion often depends on the relation between some flow parameters, and these can often be expressed as a dimensionless number or a ratio depending on the characteristics of the experiment (i.e. length scale, velocity scale etc.).

Dimensionless numbers are attractive in fluid dynamics, because some of them gives the means to compare for instance flows observed in the laboratory with flows seen in the atmosphere. If the naturally occurring phenomenon and the experiment in the lab have the same dimensionless numbers attached they should exhibit the same physical behavior in spite of the very different absolute length and velocity scales. Obviously, not all dimensionless numbers have this property, so choosing the right one often gives important insight into which physical phenomenon is the most dominant in the experiment.

In this experiment, the following key parameters are at hand to construct dimensionless numbers: The radius of the cylinder,  $R$ , the water level,  $H$ , the frequency of the rotating lid  $\Omega$  and, the viscosity of the fluid  $\nu$ . Besides that, a number of other parameters such as the surface tension and the gravitational acceleration could also be used, but we will not list them all here.

In the following sections we will present a couple of the most important dimensionless numbers in the experiment.

### 1.1.1 The Reynolds number

Defined by

$$Re = \frac{vL}{\nu}, \quad (1.1)$$

the Reynolds number gives an approximation to the ratio of inertial to viscous forces on the fluid.  $v$  denotes a typical flow speed,  $L$  denotes a typical length scale of the flow over which the velocity changes by  $v$ , and  $\nu$  denotes the kinematic viscosity.

In this experiment we will define the Reynolds number to be

$$Re = \frac{\Omega R^2}{\nu},$$

so  $v = \Omega R$  and  $L = R$  which seems reasonable.

For small values of the Reynolds number,  $Re \ll 1$  the flow creeps along slowly, whereas for  $Re \gg 1$  the flow tends to be lively.

In general there are two different types of flow: Laminar and turbulent flow, which can both be characterized using the Reynolds number. The difference between the two can most easily be explained if one considers the flow through a pipe as is shown in figure 1.2a,b

At low flow velocities, or more precisely, at low Reynolds numbers we see layered flow lines 1.2a. Different layers of fluid move with different velocities, but without exchange of particles perpendicular to the overall flow direction. This is laminar flow.

In sharp contrast to this, at higher Reynolds numbers, the fluid makes highly irregular motion perpendicular to the flow direction as shown in figure 1.2b. This is turbulent flow characterized by randomly fluctuating motion. (Lautrup, 2002,



Figure 1.2: *Flow from right to left through a pipe: a) Laminar flow ( $Re = 1150$ ), b) turbulent flow ( $Re = 2520$ ). From (Schlichting, 1999) p. 13*

Acheson, 1990) In this experiment we operate at Reynolds numbers in the range  $10^5 - 10^6$  when dealing with water and in the range  $10^3 - 10^4$  when dealing with ethylene glycol.

### 1.1.2 The Froude number

The Froude number can be described as the ratio of the square of inertial forces to the square of gravitational forces on the fluid and is defined by

$$Fr = \frac{v^2}{gL}$$

where  $v$  and  $L$  is defined as above, and  $g$  is the gravitational acceleration. There are several relevant definitions of the Froude number for this experiment depending on whether you choose  $L = R$  or  $L = H$ . We will use

$$Fr = \frac{\Omega^2 R^2}{gH}$$

as a definition of the Froude Number.

## 1.2 Fluids in rotation

### 1.2.1 A simple model: Fluids in almost solid body rotation

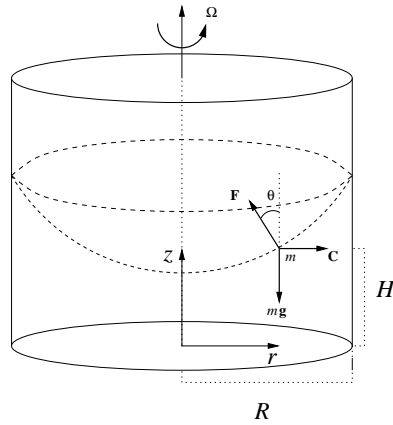


Figure 1.3: *The rotating bucket*

Our first approach to understanding the dynamics of this experiment is to consider the following simple model for the experiment; a volume of fluid in a rotating cylinder. The entire cylinder, including the bottom and walls, are rotating at the same rate, so eventually the fluid will be in solid body rotation with the cylinder.

Now, consider a small volume of fluid of mass  $m$  at the surface under rotation in a cylinder as seen in figure 1.3. In the co-rotating reference frame the forces on  $m$  is gravity,  $m\mathbf{g}$ , the centrifugal force,  $\mathbf{C} = m\Omega^2 r \cdot \hat{\mathbf{r}}$ , and the forces exerted by the surrounding fluid,  $\mathbf{F}$ . The forces from the surrounding fluid must be orthogonal to the surface of the fluid – if not,  $m$  would move tangentially which it does not since the shape of the free surface is stationary.

To compute the shape of the free surface, consider the following: Since  $m$  is stationary, we have that

$$|\mathbf{F}| \cos \theta = mg \quad \text{and} \quad |\mathbf{F}| \sin \theta = |\mathbf{C}| = m\Omega^2 r,$$

and thus

$$\tan \theta = \frac{\Omega^2 r}{g}.$$

But  $\frac{dz}{dr} = \tan \phi$  so we have that

$$\int dz = \int \frac{\Omega^2 r}{g} dr,$$

which gives us that

$$z = z_0 + \frac{\Omega^2}{2g} r^2.$$

So, in this case the free surface of the fluid has the shape of a parabola.

For sufficiently high rotation rates the fluid is pushed against the side and a jump occurs, that is, a fluid-free area of radius  $r_0$  forms in the middle of the bucket. In the moment when a jump appears we have that

$$z = 0 \quad \Rightarrow \quad r = r_0 \quad \Rightarrow \quad z_0 = -\frac{\Omega^2}{2g} r_0^2,$$

so

$$z(r) = \frac{\Omega^2}{2g} (r^2 - r_0^2). \quad (1.2)$$

Now, volume conservation gives that

$$\pi R^2 H = 2\pi \int_{r_0}^R \frac{\Omega^2}{2g} (r^2 - r_0^2) r dr = 2\pi \left[ \frac{-\Omega^2}{4g} (r_0^2 R^2 - r_0^4) + \frac{\Omega^2}{8g} (R^4 - r_0^4) \right]$$

Solving this fourth order equation, we get that

$$r_0^2 = R^2 \left( 1 - \sqrt{\frac{4Hg}{\Omega^2 R^2}} \right). \quad (1.3)$$

From this we deduce three important things. First, the size of the jump increases whenever  $\Omega$  increases, as expected. Second, the dynamical height of fluid at the rim of the cylinder is  $z(R) = \frac{\Omega}{2g} \sqrt{\frac{4Hg}{R^2}}$ , so this also increases as  $\Omega$  increases. Finally the jump first occurs at the frequency  $\Omega = \sqrt{\frac{4Hg}{R^2}}$ . Besides that, we note the appearance of the dimensionless number  $\frac{\Omega^2 R^2}{Hg}$  which we recognize as the Froude number.

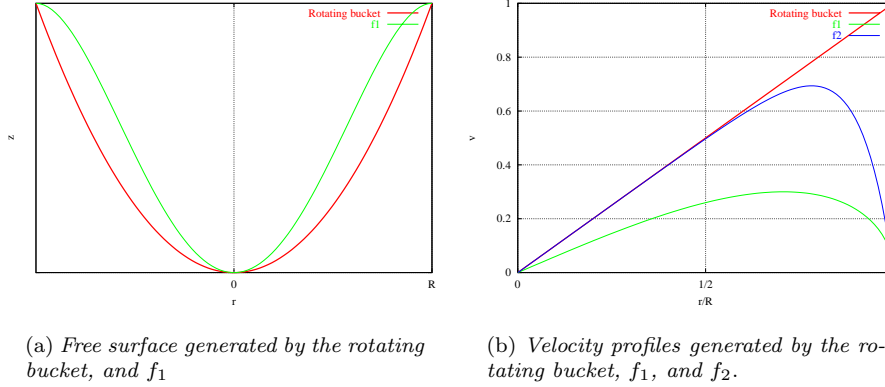
So far we have restricted ourselves to the case in which the fluid inside the cylinder is in solid body rotation along with the rest of the system. This implies that the azimuthal velocity of the fluid inside the cylinder is  $v(r) = \Omega r$ . However, in our experiment the boundary conditions dictate that  $v(r)$  must go to 0 as  $r$  approaches  $R$ . An Ansatz for  $v(r)$  would therefore be  $v(r) = \Omega r f(r)$  where  $f(r)$  is a function that fulfills the following conditions

$$f(r) = \begin{cases} 1, & \text{if } r = 0, \\ \rightarrow 0, & \text{as } r \rightarrow R, \end{cases}$$

Examples of such functions are

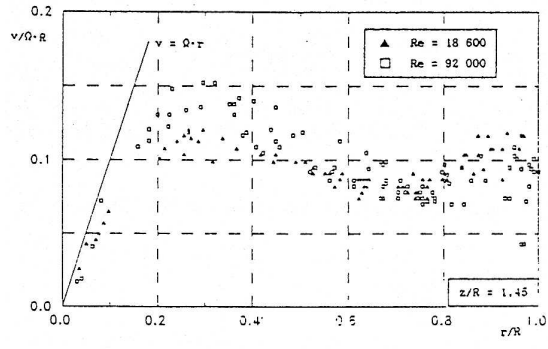
$$f_1(r) = k_1 \sqrt{1 - \left(\frac{r}{R}\right)^2}, \quad \text{and} \quad f_2(r) = 1 - e^{-k_2(1-r/R)}.$$

where  $k_1, k_2$  are some scaling parameters.



(a) Free surface generated by the rotating bucket, and  $f_1$

(b) Velocity profiles generated by the rotating bucket,  $f_1$ , and  $f_2$ .



(c) Experimental velocity profile. From (Mory and Spohn, 1992)

Figure 1.4: Velocity profiles, corresponding free surface and experimental results

Please note, that in both cases the continuity equation

$$\nabla \cdot \mathbf{v} = \frac{1}{r}(ru)_r + w_z = 0,$$

is still fulfilled.

The functions are plotted in figure 1.4(a) and are in good agreement with the experimental data seen in figure 1.4(c).

The free surface profiles generated by  $f_1$  can be seen in figure 1.4(b), where it is compared to that of the rotating bucket.

The model discussed above is a very crude model for describing the real experiment. However we expect that most of the results from above, e.g. that the size of the jump increases as  $\Omega$  increases, still holds in our experiment.

### Flow above a rotating disk

We are now going to investigate the flow above a rotating disk. The problem of describing the flow above an infinite rotating disk in a fluid was first solved by von Kármán (Kármán, 1921). The equations governing the system will not be given here, but can be found in the appendix A.1 where the solution is discussed. The

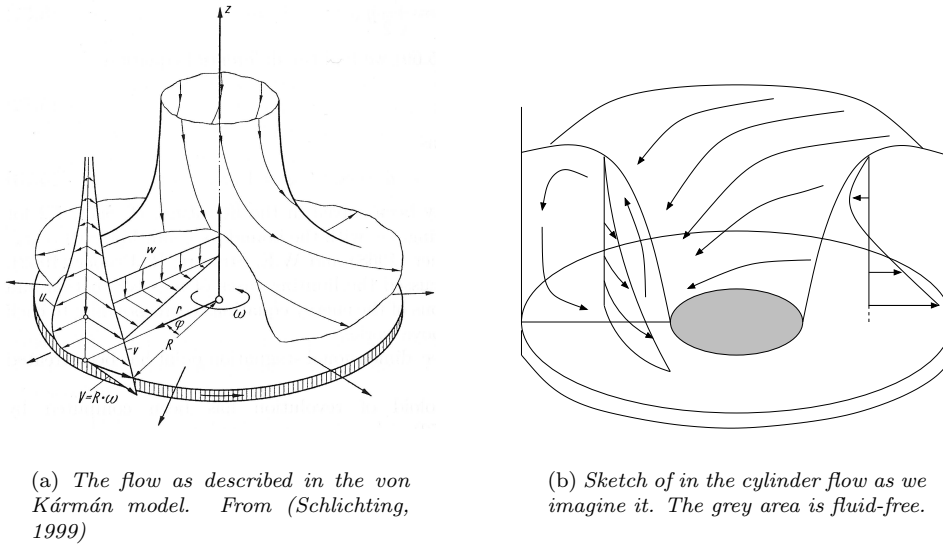


Figure 1.5: The flow produced by the von Kármán model compared to the experiment.



Figure 1.6: Shape with 3 corners seen in perspective

results of the calculations are presented in figure 1.5(a) which shows the streamlines. The viscous forces drags the fluid near the disk radially outwards under the action of the centrifugal force. The displaced fluid is replaced by some new fluid which is axially sucked into the boundary layer. The rotating disk is acting as a centrifugal pump.

When comparing the von Kármán model to our experiment, one has to keep in mind that firstly the von Kármán model is not valid in a confined geometry such as the one at hand, and secondly that the von Kármán model does not take neither the free surface effects nor the jump in the middle of the rotating fluid into account. Based purely on observations, i.e. pictures and movies, we imagine that the flow inside the fluid is as shown in figure 1.5(b). Centrifugal pumping is still observed, a fact which is also supported by (Mory and Spohn, 1992), but clearly the flow depends very much on the interaction between the different boundary layers.

# Setup and methods

In this section we first describe the technical details of the setup. Second, we will describe how we did the measurements and try to estimate the errors related to these. Finally we will discuss the methods we used when making measurements.

## 2.1 Technical description

The setup consists of a cylinder made of Plexiglas, a motor and a circular plate, placed inside the cylinder, which is rotated by the motor. The motor is an ICME Type T63BX2 electric motor and is equipped with a frequency generator T-verter N2-Series and a gearing device. The frequency generator has a counter that runs in the interval  $[0.00 : 49.00]$  in steps of 0.01, but in practice the motor can run no slower than about 7.00 due to friction. We will denote the frequency generator counter value by  $\Omega_c$ , and it is related to the frequency of the plate  $\Omega_p$  by the relation  $\Omega_p = 2\pi(\alpha\Omega_c + \beta)$  with values we have determined experimentally as  $\alpha = 0.15 \pm 0.01 Hz$  and  $\beta = -0.1 \pm 0.2 Hz$ .

### The 131 mm setup

The setup is depicted in figure 2.1(c). The cylinder has an inner radius of  $R = 131 \pm 3 mm$  and is placed on a table where 4 steel rods holds a metal plate on which the motor is mounted. 4 screws which makes it possible to adjust the horizontal alignment of the motor. An axle of length  $500 \pm 5 mm$  and radius  $14.00 \pm 0.05 mm$  connects the motor with the bottom plate. Unfortunately, the bottom plate is not placed exactly perpendicular to the axle, and the axle is only known to be vertical to an accuracy of 0.2 degrees, because we can not measure the alignment of the motor to a satisfactory accuracy. The misalignment is responsible for a vertical motion of the plate of about  $2 mm$  at the edge of the plate, which we will call the *wobbling* effect.

### The 194 mm setup

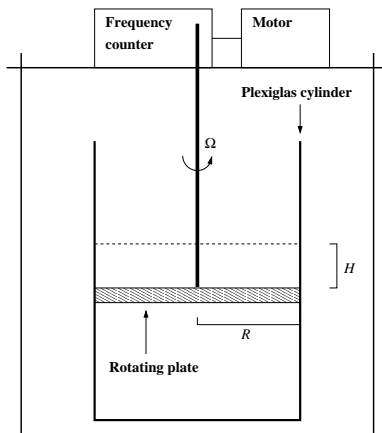
The setup is depicted in figure 2.1(d). In this setup the cylinder has a radius of  $R = 194 \pm 3 mm$  and is placed on a table and stabilized by the weight of the water and 4 wooden bricks. In this setup the same motor is mounted from below which make both experiments and observations easier. In addition, the cylinder has been provided with a tap to control the water level,  $H$ , easily. The axle goes into the bottom of the cylinder through a bearing, which makes it possible to adjust the distance from the plate to the bottom of the cylinder. However, it turned out that it was better to control the water level instead of moving the plate. The  $194 mm$  setup was much better aligned than the  $131 mm$  setup and did only show a wobbling effect of less than  $0.5 mm$ .



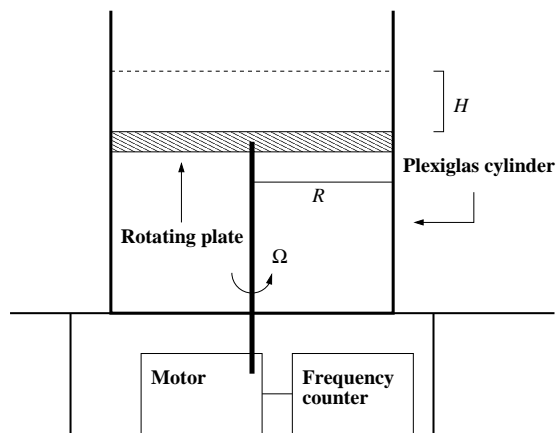
(a) *Picture, 131mm setup.*



(b) *Picture, 194mm setup.*



(c) *Schematics, 131mm setup*



(d) *Schematics, 194mm setup*

Figure 2.1: *Pictures and schematics for the experimental setups.*

## 2.2 Measurements

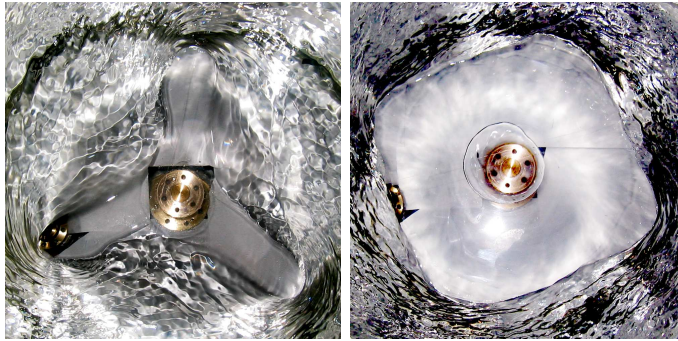
The depth of the water can be controlled in two ways: Either by simply controlling the volume of the water in the cylinder or by moving the axle. The depth is measured with a caliper to an accuracy of  $0.2\text{mm}$ , but due to the wobbling of the plate and the fact that the table is not exactly horizontal, there will always be an uncertainty of at least  $\pm 1\text{mm}$ .

We shall denote the number of corners of the shapes observed by  $k$ , and in some cases we will speak of states instead of shapes, when this is more appropriate. With this definition a  $k = 0$  shape is a circle, a  $k = 2$  shape is an ellipse, a  $k = 3$  shape is a triangle etc. (See fig. 1.1) The number  $k$  is directly observable for frequencies not much higher than the transition frequency between the  $k = 3$  and  $k = 4$  states. For

higher frequencies it is necessary to take a picture to determine  $k$ , since the shapes are rotating too fast to see with the naked eye.

For frequencies not much higher than the transition frequency between the  $k = 2$  and  $k = 3$  states, the frequency of the  $k$ -corner shape,  $\Omega_k$ , is determined with a stop watch to an accuracy of  $0.15\text{rad/s}$ . In the  $194\text{mm}$  setup it is also possible to determine the frequency of the four corner shape with the stop watch. Explicitly, we determine the frequency of a  $k$ -corner shape by counting 10 corners passing by and measuring the time it takes. We do this 3 times for each shape which gives us the mean time and uncertainty. The meantime  $t$  is related to the frequency of shapes by the relation  $\Omega_k = 2 \cdot \pi \frac{10}{t \cdot k}$ .

For higher frequencies a strobe can be used. The strobe is flashing at the water, and because the shape is rotating and the corners are almost identical, the shape will appear to be standing still in the lab frame, when the frequency of the strobe is exactly set such that it flashes every time a corner passes by. One should be aware that the shape will also appear to be standing still if the strobe flashes once for every second, third etc. time a corner passes by. It turns out to be most convenient to find the highest frequency where the shape appears to be standing still, to ensure that the strobe flashes at exactly every corner that passes by. Then, the frequency of the  $k$ -corner shape is found by reading off the strobe's frequency and divide by  $k$ .



(a)  $k = 3$

(b)  $k = 4$



(c)  $k = 5$

Figure 2.2: *Different shapes observed in the 194mm setup. Note that the 4-corner shape almost appears as a square. We have also observed a more star-like 4-corner shape as seen previously.*



(a) A 2 corner shape seen from the side

(b) A 2 corner shape seen from the front

Figure 2.3: 2 corner shape in Ethylene Glycol. The two pictures were taken within few seconds.

To check if the shape is phase locked the strobe is set in such a way that the plate appears to be standing still in the lab frame. This can be done in the 131mm setup, because the plate has marks that indicates the rotation. The frequency of the figure is locked to that of the plate with a rational factor if and only if the shape also appears to be standing still.

Note that these measurements are very unpleasant because the strobe is the only light in the lab, and one should be aware of not making too many measurements without pause. Hence, we preferred to use the stop watch, since the uncertainties of these measurements were satisfactorally small.

### 2.3 Experimental method and observations

When conducting the experiment two parameters can be controlled. First, the water level is set to the desired value. Second, the frequency of the motor is set to approximately  $1Hz$ , which is the lowest possible frequency, and the frequency is thereafter increased in small steps of about  $0.1Hz$ . This method is necessary to follow, since it turns out that hysteresis is evident in the setup – we shall return to this in more detail later. Furthermore, it is necessary to increase the frequencies in small steps, since some of the states only exists in very narrow frequency intervals. In addition to this, the system sometimes need some seconds to stabilize.

We will now go through the series of events that occur as the frequency is increased. When the frequency is set to the starting frequency of about  $1Hz$ , we observe either a  $k = 0$  or a  $k = 2$  shape, all depending on the water level. It should be mentioned, that the state is very difficult to determine for such low frequencies because the deformation of the surface is not very large.

As the frequency is slowly increased, the  $k = 2$  shape eventually becomes clearly visible because the deformation of the surface gets larger. In addition, the surface comes closer to the plate. For some certain frequencies and water levels the system is seen to oscillate between 2 or more states. It is even seen to oscillate between the two types of sub states  $a$  and  $b$ , where  $a$  denotes the sub state in which the free surface reaches the plate and  $b$  denotes the sub state in which the free surface does not reach the plate, i.e. the plate is completely covered by water.

As the frequency is increased further, the  $k = 2$  state becomes more unstable and the shape of the surface becomes irregular. When the frequency reaches the transition frequency between the  $k = 2$  and  $k = 3$  states, the shape of the surface



Figure 2.4: *Intermediate state between a  $k = 3$  and a  $k = 4$  shape. This particular shape is regarded as a highly irregular  $k = 4$  shape, since the fourth corner has just developed, but is still not stable. Although states like this occasionally appear near the transition states, the vast majority of the shapes observed are regular.*

is either irregular and it is difficult to determine if it is a  $k = 2$  or  $k = 3$  shape or it finds an intermediate  $k = 0$  state.

Near the transition frequency, typically within  $0.3Hz$ , the states are unstable, and it is usually possible to observe  $k = 2$  as well as  $k = 3$  states at the same frequencies depending on whether the frequency is changed from lower frequencies to higher frequencies or vice versa.

This overall behavior repeats itself for the  $k = 3$ ,  $k = 4$  states and so on, though there are some variations. As an example a  $k = 3$  state is seen to oscillate between  $k = 0$  type  $a$  and  $b$ , and  $k = 3$  type  $a$  and  $b$  states – all together four distinct states. It should also be noted, that the frequency interval, in which a particular shape exists, gets narrower as  $k$  increases.

In general we can say that  $k$  increases whenever frequency increases and  $k$  decreases when the water level is raised.

# Results

In this section we will present the results obtained as explained in Setup and methods. We started out using the 131 mm setup and later on the somewhat bigger 194 mm setup. Both is depicted in figure 2.1. The 194 mm setup provided the means for making a second phase diagram to verify earlier results, taking better pictures and making movies since the axle is mounted from below.

Below we present our results in the following order. First we present the phase diagrams, showing at which water levels,  $H$ , and plate frequencies,  $\Omega_p$  or  $f$ , the different shapes occur for both the 131 mm and the 194 mm setup. Next we present the results of our investigation of the phase locking of the rotating shapes. This is interesting since when a  $k$ -shape occurs in the free surface the frequency,  $\Omega_k$ , with which it rotates relative to the lab frame is different from that of the plate. After that we present the results about hysteresis. The system apparently has the property that going from low to high plate frequencies is not quite the same as going from high to low frequencies.

Motivated by (Spohn et al., 1993) we then turn to investigate the effect of changing various key parameters in the experiment, and thereafter we discuss the effect of these perturbations on the stability of the shapes. Finally we look at some of the different states of the system, and the transitions between these.

## 3.1 Phase diagram

One of the main results of this project is the construction of the phase diagrams. They can be seen in figures 3.1 and 3.2. The phase diagrams show the number of corners  $k$  as a function of the water level,  $H$ , and the frequency of the rotating plate,  $f$ . As it is seen they group together, some in islands and some in larger areas that seem to stretch beyond the scale of the phase diagram produced.

There are some transition states where a  $k = 0$ -state occurs between e.g. a  $k = 2$  and a  $k = 3$ -state. This phenomenon is not solely due to the fact that the shape became highly distorted in the transition states — sometimes stable  $k = 0$  states appeared between two states.

### 3.1.1 Water in 131mm container

The phase diagram is build from 676 data points collected by slowly increasing the frequency for a given height – hence, the data is seen as vertical lines. The phase diagram was done with water in the cylinder of radius  $131 \pm 3mm$ . We did a sample run of the experiment before we made the actual diagram, so we knew roughly where to find the different states. Therefore we started the experiment at the height just before the first shapes appeared, and we stopped at the height where water would come over the side if we turned the plate too fast.

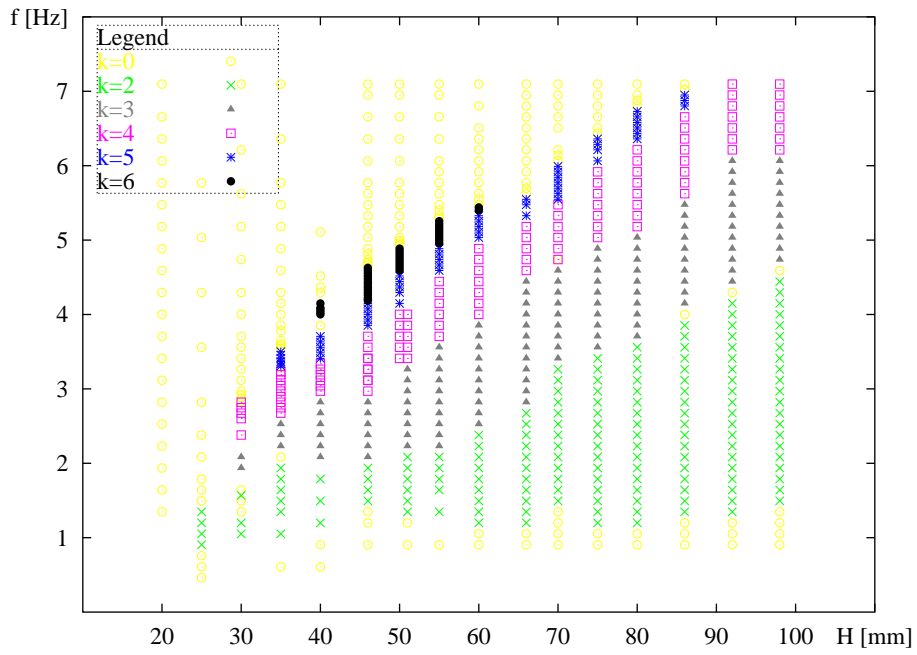


Figure 3.1: Phase diagram for the 131 mm setup with water.

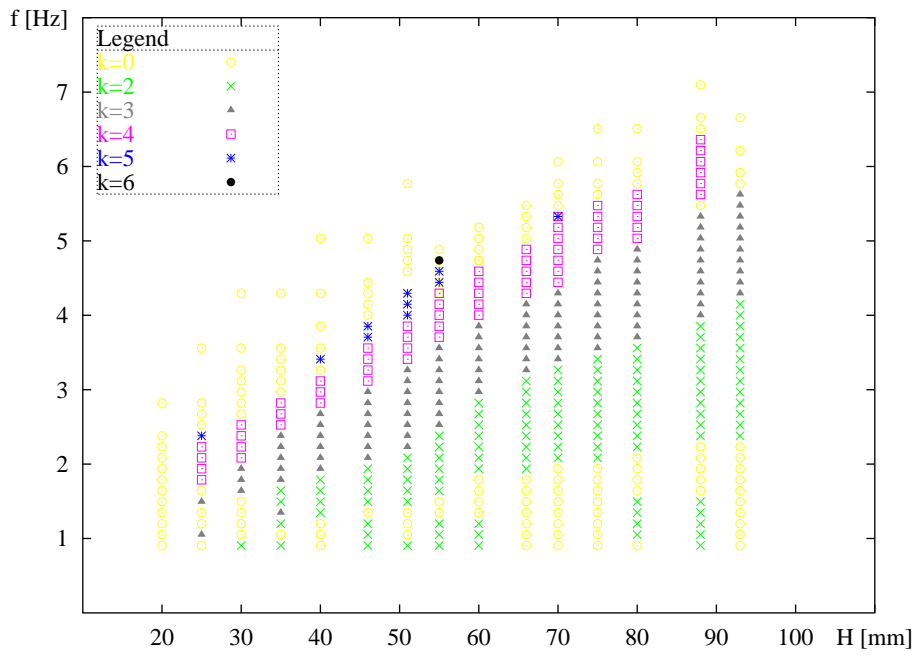


Figure 3.2: Phase diagram for the 194 mm setup with water.

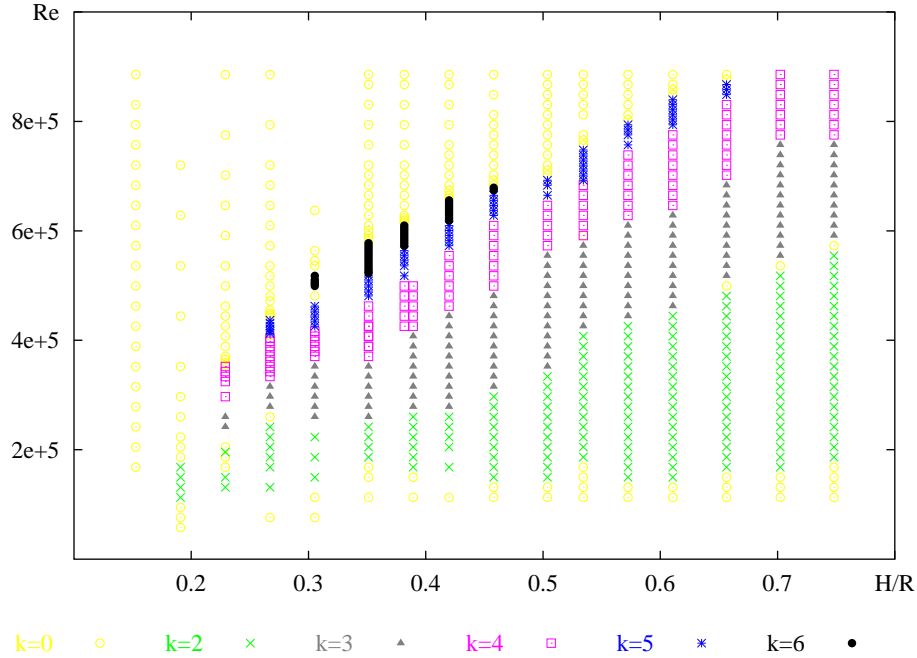


Figure 3.3: Phase diagram for the 131 mm setup with water plotted using the Reynolds number and the aspect ratio  $H/R$ .

### 3.1.2 Water in 194mm container

The phase diagram for the 194mm setup was done in the same manner as the 131mm setup, and it is made from 447 data points. The 194mm setup was able to contain more water, so we were able to make the phasediagram for the same values of the aspect ratio  $H/R$  as in the old 131mm setup. Unfortunately, due to overheating caused by friction in the bearing, the 194mm setup could not be run at high driving frequencies for longer periods of time. So, since high frequencies are needed to see the shapes for large  $H/R$ , we were only able to make the experiment for the same values of  $H$  as in the 131 mm setup.

If the two phase diagrams are compared, several observations can be made. First of all, the overall structure and appearance of the the two phase diagrams are very similar. The  $k$ -states follow the same pattern on both figures, and the same islands of  $k$ -states occur at roughly the same places. Another similarity is that for the same water level, the  $k$ -states appear at roughly the same frequencies in the two setups. This is somewhat surprising, because it indicates that the cylinder radius,  $R$ , is in fact not a crucial parameter in the experiment. We shall discuss this later in greater detail; but from now on we will plot the data using the absolute height,  $H$ , instead of the aspect ratio,  $H/R$ , which has been used elsewhere (Mory and Spohn, 1992). The main difference between the two phase diagrams is that in the 194 mm setup we have made fewer observations of states with higher  $k$ -numbers. This indicates that somehow it gets more difficult for the surface to form shapes with many corners with increasing  $R$ .

The transitions between different  $k$ -states in the two phase diagrams for water and the one for ethylene glycol are shown in figure 3.8. It is seen that the transitions follow straight lines and that these lines are roughly equal for the two setups in water. We shall return to a further discussion of this diagram later.

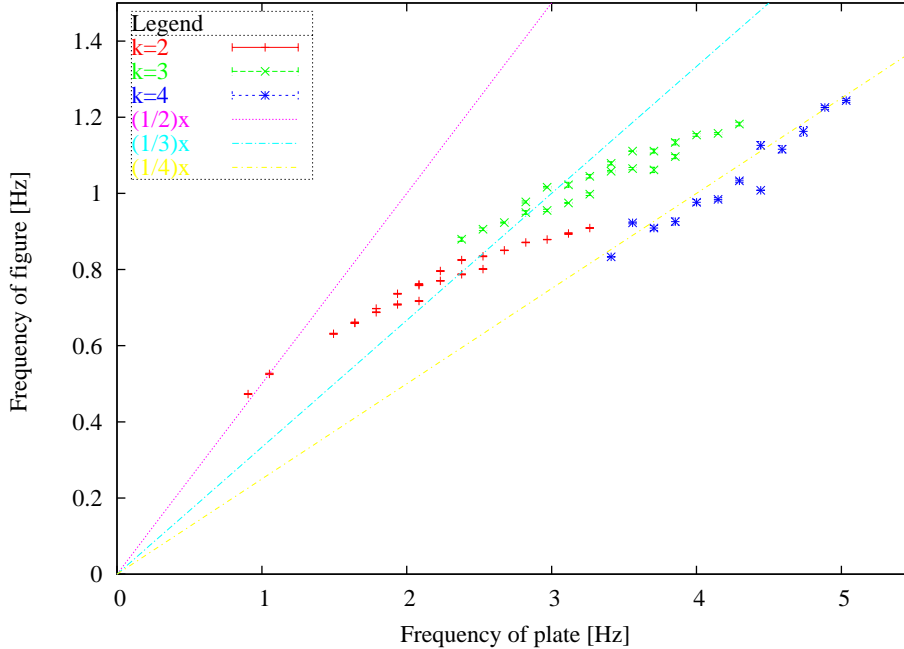


Figure 3.4: Frequency of the  $k$ -shapes as a function of the frequency of the bottom plate for the 194mm setup.

## 3.2 Phase locking

We have investigated the frequency of the  $k$ -shapes,  $\Omega_k$ , as a function of the frequency of the bottom plate,  $\Omega_p$ . The data was collected for the heights 51mm, 60mm and 70mm in the 194mm setup. These were chosen due to the large amount of ellipses, triangles and squares. The results are plotted in figure 3.4.

We had hoped for a simple relation for the phase locking like  $\Omega_k = \frac{1}{k}\Omega_p$ . The  $k = 2$  state follows the line with slope  $\frac{1}{2}$  for the first two measurements, but then deviate considerably making it difficult to determine whether or not it is locked by a factor of  $\frac{1}{2}$ ,  $\frac{1}{3}$  or if it is locked at all. The slope of the  $k = 3$  state follows the line with slope  $\frac{1}{3}$  for the first few measurements, but as before it is hard to determine the actual locking parameter, if any. It is seen that the  $k = 4$  state follows the  $\Omega_4 = \frac{1}{4}\Omega_p$  line, giving the strongest indication that phase locking is occurring.

## 3.3 Hysteresis

While making the measurements it turned out that at least two different  $k$ -states can be observed for the same plate frequency. We found two ways to make the system relax into different states for the same frequency. First, when frequency is changed in sufficiently large steps ( $\geq 1Hz$  or so) and second, when turning the experiment around i.e. starting the experiment at high frequencies which is then decreased.

The frequencies for which two different states can be observed is usually near the transition frequency between two states, as seen in figure 3.12(d). The  $k$ -states are not very stable around these transition frequencies, so it is not very surprising that the system can end up in either one of the two states when the frequency is altered in big steps.

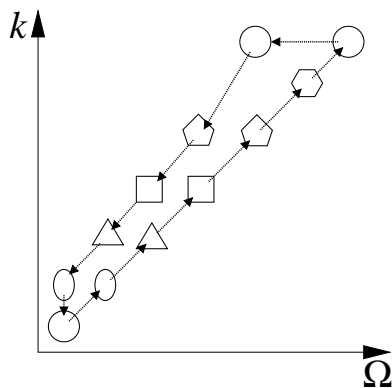


Figure 3.5: Schematics of the hysteresis observed in the system. Coming from different (frequency) directions makes it possible to have more than one  $k$ -state for each  $\Omega_p$ .

Starting at the highest possible plate frequency ( $\sim 7.25Hz$ ) and then decreasing the frequency in steps of  $0.15Hz$  is a reversal of the experiment. It is a bit of a surprise that the system is behaving differently in the two situations. Figure 3.12(d) indicates that some hysteresis is evident in the system, but we can not tell if it is due to the imperfections in the setup or if it is an intrinsic feature of the system. Figure 3.5 shows schematically the hysteresis we observe.

### 3.4 The effect of changing key parameters in the experiment

#### 3.4.1 Substituting water with Ethylene Glycol

To investigate the experiments dependence on viscosity, we filled the 131 mm cylinder with ethylene glycol, which has a kinematic viscosity  $\nu$  about 20 times greater than that of water (D. R. Lide, 1995). Thus, since  $Re$  goes as  $\frac{1}{\nu}$  we expect the same flow characteristics in the experiment at frequencies 20 times less compared to the experiment with water. As the motor runs very badly at frequencies less than about  $1Hz$ , which corresponds to  $Re = 6,300$  in ethylene glycol. From the phase diagram (figure 3.3) we should expect to observe nothing but the  $k = 0$  state. However, as seen in the figure 3.11, surprisingly we also observe the  $k = 2$  and  $k = 3$  states. This is not quite what we expected, since it seemed reasonable to expect the Reynolds number to be the characteristic number of the system.

Instead of the Reynolds number, we might assume that the Froude number, as previously described, could be the characteristic number for the system. Figure 3.11(b) indicates that it would be a slightly better idea to use  $Fr$  instead of  $Re$ , but the results are not quite satisfactory.

We have tried a number of other dimensionless numbers as well, but none of them gave a better result. So, since  $H/R$  is not a good number either, we have decided to simply plot everything in raw data — i.e. frequency against water level instead of using the Reynolds or Froude number. Surprisingly, as seen in figure 3.11(c), this gives good agreement between the water and ethylene glycol measurements, indicating that the absolute length scale and frequency is of some use for comparison.



Figure 3.6: A triangle in ethylene glycol, as seen on the front page. Notice the clearly visible vortices in the flow direction.

### 3.4.2 Changing the surface tension

To investigate the influence of surface tension in the experiment we added  $5 \pm 0.2ml$  of concentrated washing up liquid to the water. giving a total concentration of washing up liquid of 0.05 %. The choice of  $51mm$  was made due to the fact that this height exhibit all the different shapes and a change would be easy to observe. Changing the surface tension had an influence on our experiment. In figure 3.12(a) it is seen that the most of the states still exist, but has moved to lower frequencies. Please note that ethylene glycol also has a different surface tension than that of water, but that this experiment was made to isolate the effect.

### 3.4.3 Misaligning the cylinder

We tried deliberately to misalign the cylinder to see if a misalignment in our setup was the cause of the symmetry breaking observed. Two kinds of misalignments were tried. First, the cylinder was tilted by an angle of  $\theta = 1.3$  degrees, as seen in figure 3.7(b). We did the experiment for  $H = 55mm$  in the  $131mm$  setup. As seen in figure 3.12(b) no differences was evident within the uncertainty.

Second, the axle was misaligned by  $\theta = 1.0$  degrees, as seen in figure 3.7(a), and nearly no effect was observed as seen in figure 3.12(c).

## 3.5 Stability and time evolution of the states

In this section we want to describe the time evolution and the stability of the different kinds of states we observe. First we note that the number of corners  $k$  increases when  $\Omega_p$  is increased (see figure 3.1). If a  $k$ -state exists in a given interval of frequencies, the most stable states are observed close to to the middle of this interval. The most stable states are stable to quite large mechanical perturbations,

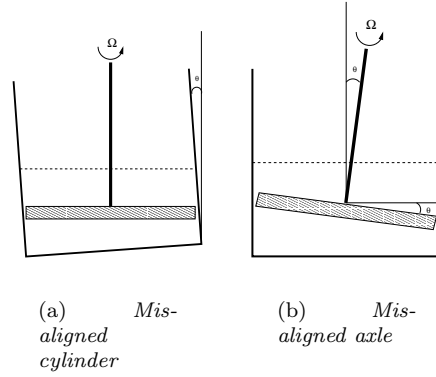


Figure 3.7: *Deliberately misaligned setups.*

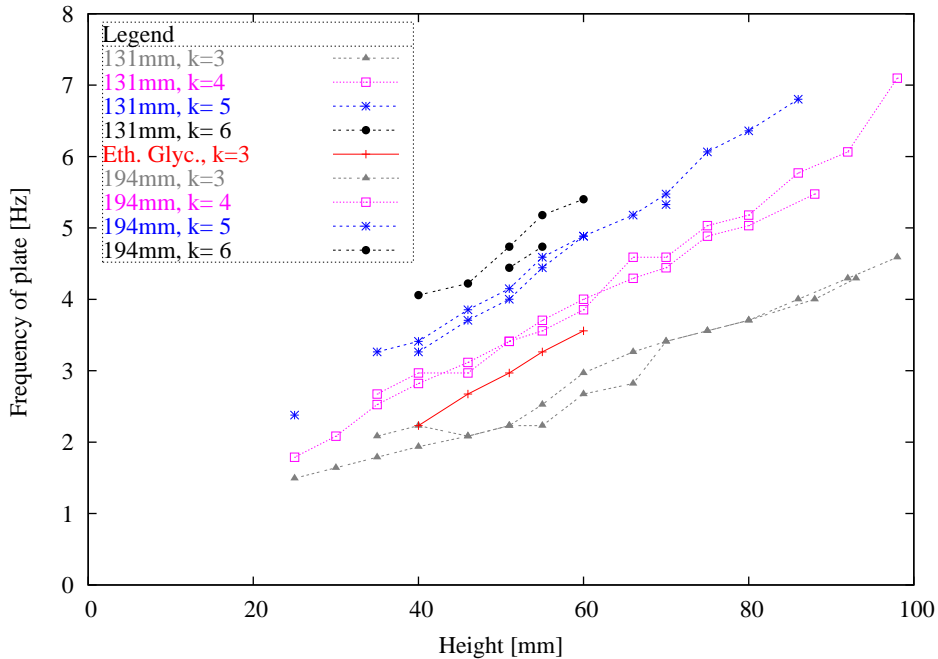


Figure 3.8: *Transition between  $k$ -states for the 131mm setup, the 194 setup and the ethylene glycol measurements. The  $k$ -valued lines indicate the first appearance of the  $k$ 'th state.*

such as holding a ruler into the water. Even larger perturbations slow down the water considerably, and hence the stability is decreased. If the perturbation is great enough, the system is seen to go to the  $k = 0$  state. When the perturbation is removed, the stable systems returns to the  $k$ -state a few seconds after the water has regained its velocity. See figure 3.9 for an example of a stable  $k = 3$  state.

When the frequency is getting close enough to the endpoints of a given interval of frequencies, the  $k$ -state becomes unstable. Hence, even a small perturbation can kick the system out of the  $k$ -state, and the system does not return to that state. Instead, if the frequency is close to the upper (lower) bound of the interval, the new state of the system is either a  $k_{new} = 0$  state or a  $k_{new} = k_{old} + 1$  ( $k_{new} = k_{old} - 1$ ) state. For some states, the  $k_{new} = 0$  state is seen to become unstable and decay to

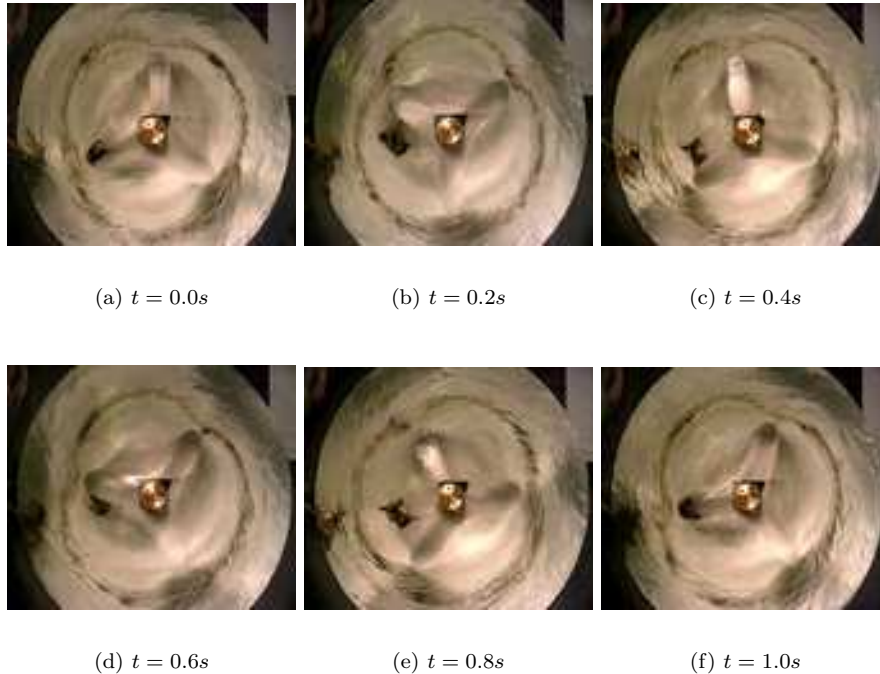


Figure 3.9: *Time development of a steady rotating  $k = 3$  shape. As it is seen the shape has a frequency of about 1 Hz relative to the lab. The plate frequency is about 3 Hz, and the camera is fixed in the lab.*

the  $k_{new} = k_{old} + 1$  ( $k_{new} = k_{old} - 1$ ) state after a few minutes, which corresponds to about 500 – 1,000 revolutions of the plate.

For  $H = 52 \pm 1mm$  and a stable  $k = 3$  state at a frequency  $\Omega_c = 19.50$  we have let the experiment run for 67 minutes without observing any changes.

It should be noted that not all transitions follow this pattern. We have seen some examples of states that change within a very narrow frequency band. Consider figure 3.10. The system started out in a stable  $k = 0$  state. At the time  $t = 0$  the frequency is increased by  $0.15Hz$ , and eventually after  $20s$  the frequency of the water has increased to the frequency corresponding to the new frequency of the plate. Look at the times beneath the pictures and note how rapidly the state changes to a stable  $k = 2$  state and note how the water raises  $4cm$  in the center of the cylinder.

Furthermore, some meta stable states are observed. For some values of  $H$  the system is observed to oscillate between two, three or even four different states. Mostly the system oscillates between two neighboring states, i.e. between the  $k = 0$  and the  $k = 2$  state etc., but sometimes the system can be seen to oscillate between the  $k = 2a$  and  $k = 2b$  states etc., where  $a$  denotes the sub state where the plate is completely covered by water, and  $b$  denotes the sub state where a part of the plate is free of water. For a few values of  $H$  the system is seen to oscillate in a four-cycle. For example, for  $H = 70 \pm 1mm$  and  $\Omega_c = 24$  the system oscillates in the cycle ( $0a \rightarrow 0b \rightarrow 3b \rightarrow 3a$ ). The period of these oscillations are typically of the order of 60 revolutions of the plate, the four-cycle having a period of about  $2 \cdot 60$  revolutions of the plate.

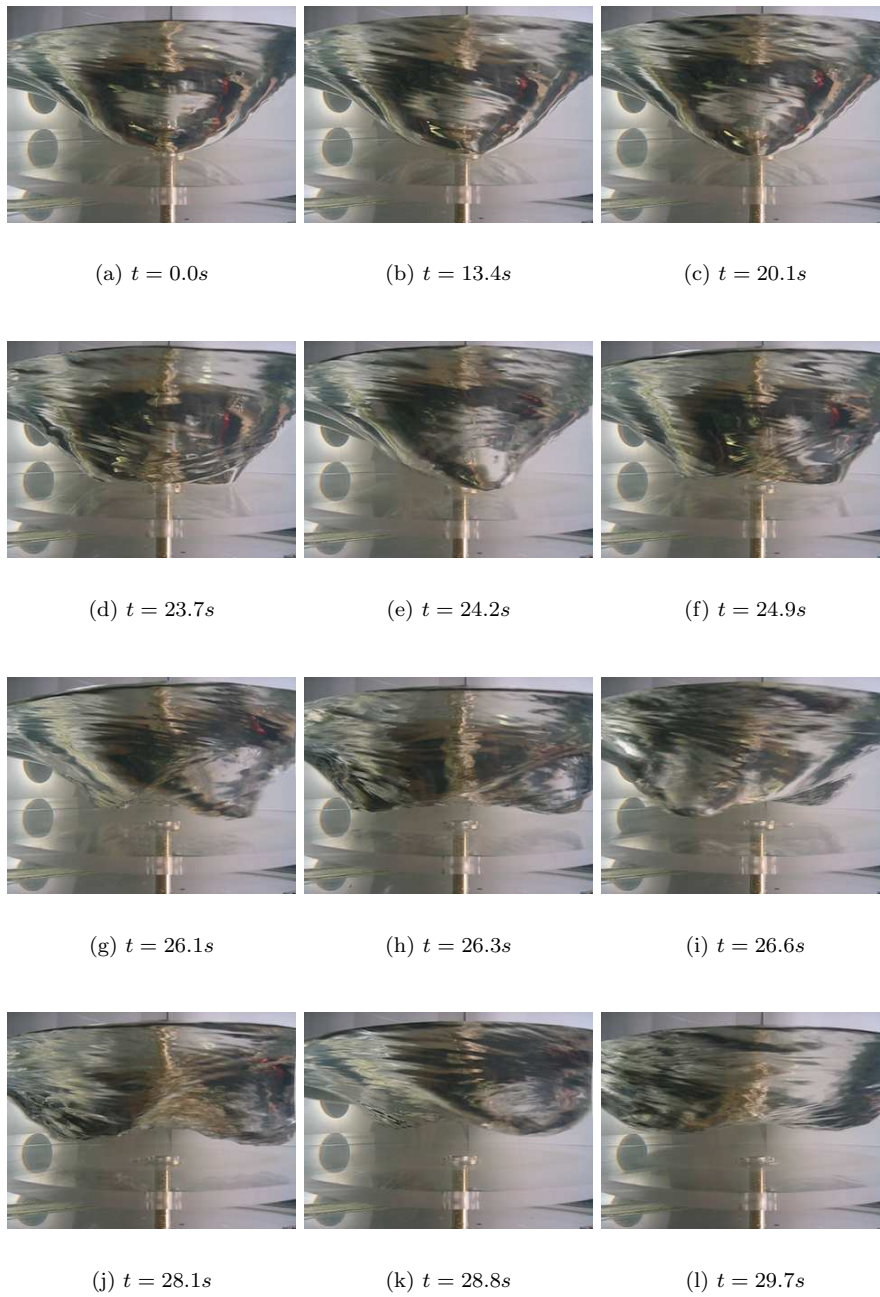
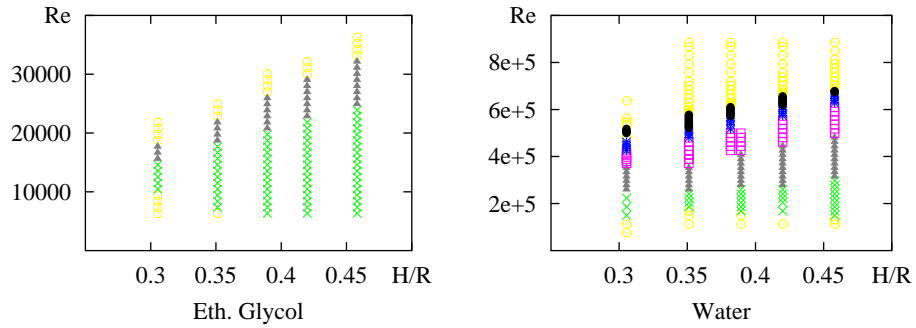
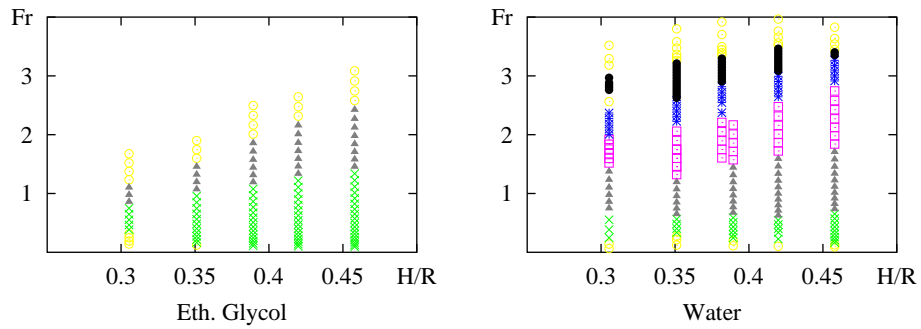


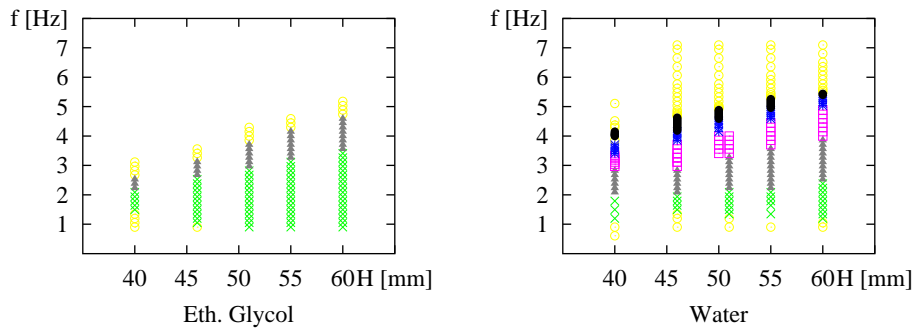
Figure 3.10: Time development of a transition between a  $k = 0$  state and a  $k = 2$  state. At  $t = 0$  the frequency is increased from  $2.30\text{Hz}$  to  $2.45\text{Hz}$ . The water level is  $93\text{mm}$ .



(a) *Eth. glycol and water compared with frequency against aspect ratio.*

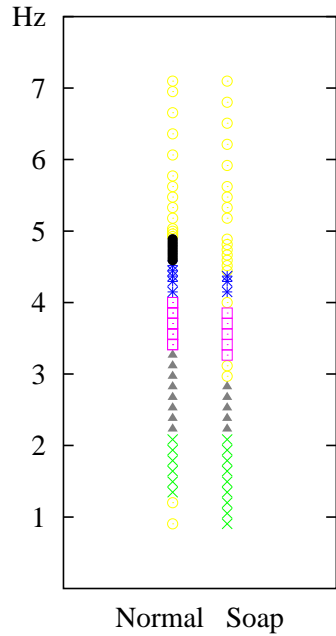


(b) *Eth. glycol and water compared with Froude number against aspect ratio*

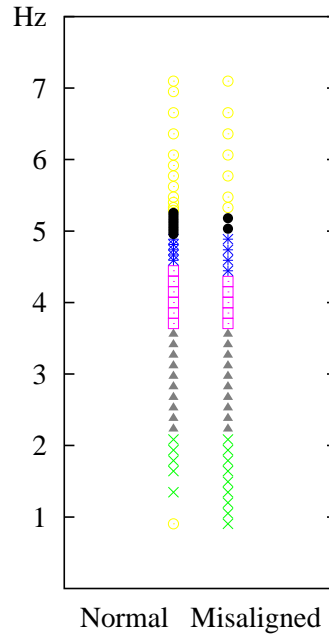


(c) *Eth. glycol and water compared with frequency against water level*

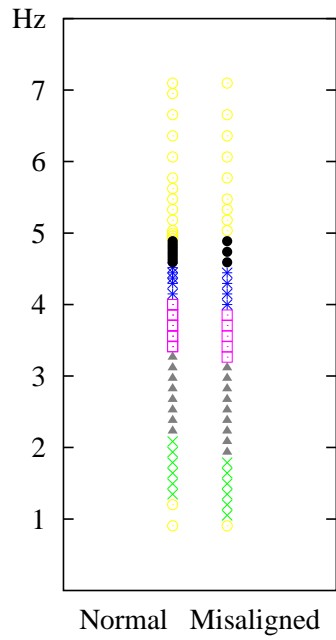
Figure 3.11: Comparison of experiments made with ethylene glycol and water in the 131 mm setup with the same aspect ratios: 0.30, 0.35, 0.38, 0.41, 0.45. We can see that the Reynolds numbers does not provide a good dimensionless number for describing the system. The Froude number  $Fr$  does provide some means for comparison. We have removed  $k = 0$ -states above  $Fr = 4$ .



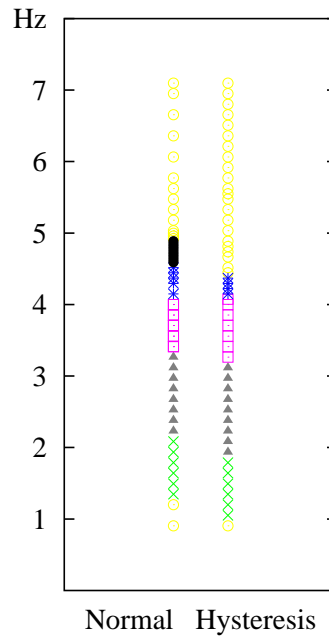
(a) Soap,  $H = 51\text{mm}$



(b) Misaligned cylinder,  $H = 55\text{mm}$



(c) Misaligned axle,  $H = 51\text{mm}$



(d) Hysteresis,  $H = 51\text{mm}$

Figure 3.12: All the perturbations compared to the unperturbed water system in the 131 mm setup at same water levels. (a) Difference in the occurrence of shapes when decreasing the surface tension. (b) Effect of a forced misalignment of the cylinder of 1.3 degrees. (c) Effect of a forced misalignment of the axle of 1.0 degrees. (d) "Normal" corresponds to the experiment made with increasing plate frequency. "Hysteresis" corresponds to the experiment made with decreasing plate frequency.

# Discussion

We will first discuss the results presented earlier and then draw some conclusions if possible. Second, we will discuss some loosely formulated ideas of an explanation of the phenomenon. Furthermore we will compare our experiment to other experiments that have revealed similar phenomena. Finally we will present a small group of subjects which we think could be interesting to study further.

## 4.1 Discussion of the results

### 4.1.1 Phase diagram

It is interesting to compare the phase diagram we constructed with the one made by (Mory and Spohn, 1992), which can be seen in figure 4.1. Comparing that to figure 3.3 we see that even though the  $Re$  and  $H/R$  domains are very different there are still some similarities. E.g. the different states occur in similar domains in both figures.

For clarity, we should note that whereas we treat the symmetry breaking in the free surface, the states described in figure 4.1 corresponds to internal symmetry breaking in the mean flow.

### 4.1.2 Symmetry breaking, viscosity, and the Reynolds number

The idea of making the experiment with ethylene glycol was to test if the symmetry breaking is a viscous phenomenon or if some other mechanisms were responsible. The work that has been done so far concerning rotating fluids, although most of it has been done for low Reynolds numbers, has revealed insight to the symmetry breaking and the flow is quite well understood with the Reynolds number as the characteristic number for the flow.

Therefore we expected the Reynolds number to be an important parameter in our system, or actually *the* characteristic number for the system together with the water level  $H$  or aspect ratio  $H/R$ .

Had the Reynolds number been the characteristic number of the flow, we would expect to find the same shapes in ethylene glycol at the same Reynolds numbers as we found them in water. Because  $Re \propto \frac{\Omega r}{\nu}$  and  $\nu_e$  is, say 20 times greater than  $\nu$ , the frequency for which the shapes exist should be 20 times less than for that of water. But since the setup cannot operate at such low frequencies, we did not expect to see any symmetry breaking in the ethylene glycol at all.

Surprisingly it turned out, that the shapes in ethylene glycol appeared in roughly the same frequency domains as for water (see fig. 3.11(c)). Large difference between the two experiments is seen, but the difference in frequency is less than a factor of two, while the difference in Reynolds number is more than a factor of 10.

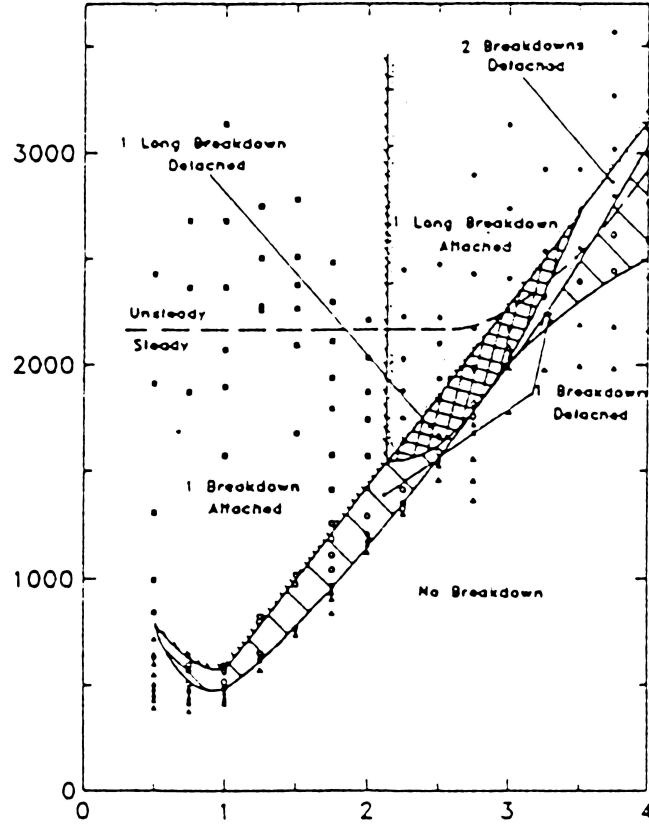


Figure 4.1: Phase diagram made by Mory and Spohn. It shows the internal flow symmetry breaking in a system similar to ours. From (Mory and Spohn, 1992).

It should be noted that surface tension should also be taken into account, since ethylene glycol has a surface tension of about two thirds of that of water (D. R. Lide, 1995), but according to figure 3.12(a) this should not effect the experiment nearly as much as we expected the Reynolds number to do. Another thing that might effect our results is the fact that there is some uncertainty in the value of the viscosity of the ethylene glycol, because the viscosity of ethylene glycol tends to decrease when in contact with air due to absorption of water vapor. Hence, the effect of using ethylene glycol instead of water should not be as pronounced as the figure 3.11(a) indicates. Still, it is far from the result we expected.

### Further discussion of the Reynolds number

In the case of our setup comprising of a fixed cylinder of radius  $R$  with a rotating bottom plate of frequency  $\Omega_p$  a typical flow speed could be  $R\Omega_p$  (i.e. the azimuthal velocity of the rotating bottom plate at  $r = R$ ), and a typical length scale could be  $R$ . Equation 1.1 thus becomes

$$Re = \frac{R^2\Omega_p}{\nu}. \quad (4.4)$$

This clearly shows the subtlety of the definition of the Reynolds number in that it is far from certain that the fluid, actually moves with a mean azimuthal velocity

$R\Omega_p$ . A more relevant definition of the Reynolds number in this context is

$$Re := \frac{v_{\text{mean}}R}{\nu} = \frac{\int_0^R v(r)dr}{R} R, \quad (4.5)$$

where  $v(r)$  is the radial velocity profile of the fluid representing the azimuthal velocity  $v$  as a function of the radial distance  $r$ .

In reality, the velocity profiles of fluids in confined cylindrical geometries depends on a number of parameters; e.g.  $H/R, \omega, \nu$ , the boundary layer thickness and the surface tension, so one has to be very careful in comparing flow characteristics of different fluids based solely on Reynolds numbers found by using equation 4.4.

While the Reynolds number describes the viscous properties of a fluid, the Froude number provides a kind of description of the the inertial properties of the fluid. That is, if the Froude number is the characteristic dimensionless number of the fluid, other mechanisms such as gravity waves might be responsible for the phenomena we observe.

### 4.1.3 Aspect ratio and the water level

With the new  $194mm$  setup we were able to test the system's dependency on the aspect ratio,  $H/R$ . Intuitively we expected to find the same states in the new setup if the frequency was the same and  $H/R$  was the same as in the  $131mm$  setup. One could argue that we should not use the frequency but instead use the Reynolds number, which should be the same if we were to expect the same distribution of the states. But since the discussion above indicates that the Reynolds number is not the characteristic number of the system, it does not seem reasonable to use. After all, the experiments show that this is not the case.

Surprisingly, we observed the same figures in the  $131mm$  and  $194mm$  setup for almost the same absolute water levels. This indicates that the experiment is not or very little dependent on the radius of the cylinder. Of course, this can not be true for very large and very small  $R$ , but it is quite interesting that the size of the cylinder does not effect the experiment much, at least in the domain we are working. This leads us to plot our data against  $H$  instead of  $H/R$  which was our first intention since it is a dimensionless number.

### 4.1.4 Transitions between different states

In figure 3.8 we show the transition lines between the different  $k$ -states for the  $131mm$  setup, the  $194mm$  setup and the ethylene glycol experiments. Within the uncertainties of the measurements, not much qualitative difference between the  $131mm$  setup and  $194mm$  setup is seen. First, it seems reasonable to fit straight lines to each of the transitions of each experiment, and second these transition lines between the  $k = 2$  and  $k = 3$  states in the  $131mm$  setup has roughly the same slope as the corresponding transition line in the  $194mm$  setup and so forth.

If, however, figure 3.8 was plot against  $H/R$  instead of  $H$ , it is clear that the transition lines would have different slopes, and that is what we mean by saying that  $H/R$  is not a characteristic number of the system. That is, we do not make the same observations for same  $H/R$ , but we do indeed for same  $H$ .

### Surface tension

An explanation to why we see less states when adding soap to the water is that soap has the ability of decreasing the surface tension of the water. This might mean, that it will become more difficult for the water to maintain the shape of the

surface, especially sharp corners. The more corners there is in a shape, the sharper the corners must be because they get squeezed together.

Since the surface tension is smaller, the states get unstable for smaller  $k$  and hence we will not expect to find all states if the surface tension is changed sufficiently.

### **Misalignment of the cylinder**

We have not had the opportunity to make experiments in the same controlled environments as done in (Spohn et al., 1993) and even though it has been shown in a numerical computation of somewhat same character (Thompson and Hourigan, 2003) that the influence of these misalignments are able to create the main details of non-axis symmetric open breakdown bubbles, we find that these misalignments have hardly any influence. We tried to increase the misalignments to estimate the effects of this. However, from this we can not say anything about the difference between a perfectly aligned setup and the setup with a small misalignment. Even though there is a small misalignment in the setup, it will lead to a forced symmetry breaking, while spontaneous symmetry breaking is only observed in a very well aligned experiment (Hirsa et al., 2002) p. 29.

### **4.1.5 Rotating vortices**

When an a-sub state, i.e. the sub state which is not touching the plate, is observed, the corners are seen to be a bubble of air which is pressed into the surface of the water. These bubbles looks in much the same way as if there was a vortex in each corner, but it is not easy to see the real behavior of the flow without measuring the velocity field.

However, we have observed the flow near the corners in a four corner shape, where the frequency was such that the corners was just above the plate. It turned out that in front of each corner there was a rapidly rotating vortex (see figure 4.2). It seems reasonable that around each corner in an a-sub state there should be a vortex, which is responsible for the deformations of the free surface that we regard as corners. But what happens when the frequency is increased and the shape eventually reaches the plate? The vortex can not continue rotating under the corner, simply because there is not water all way around.

What we think happens is that while the corner comes closer to the plate, the vortex moves in front of the corner, and eventually settles down at the side of the shape. So, when the corners finally touches the plate, the vortices are lying at the sides of the shape, a bit like the balls in a bearing, rotating in the same direction as the plate.

There has been done some modeling of rotating vortices in a circular domain, but it reaches beyond the scope of this project to investigate in further detail whether or not the shapes we observe can be modeled with rotating vortices.

## **4.2 Other work of interest**

### **4.2.1 Other experiments concerning cylindrical flows**

As mentioned in the introduction, various types of symmetry breaking in rotating fluids has been known for some time e.g. (Lopez et al., 2003), but none of them are really comparable to this experiment, mainly because of the big difference in rotation rates.

In (Lopez et al., 2003) the experiment they observed a qualitative difference in the mechanisms leading to symmetry breaking in shallow ( $H/R = 0.25$ ) and deep ( $H/R = 2.0$ ) systems respectively. The experiment was carried out for Reynolds



Figure 4.2: *A four corner shape with a vortex just in front of each corner.*

numbers in the order of  $10^3$ , and it should be noted that the radius of the cylinder was  $25\text{mm}$ , which might increase  $R$  dependence of the system.

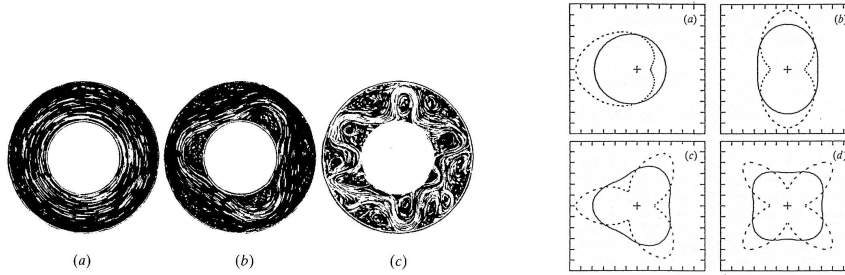
Three different modes of waves were observed, which have the same symmetries as the  $k = 2$  to  $k = 4$  shapes we have observed. Still, we can not say if it is the same mechanisms that lead to symmetry breaking in our experiment, because it has been carried out in completely different domains of both length scales as well as Reynolds numbers. Also, what is described in (Lopez et al., 2003) is not the same spectacular phenomenon, since for the deep systems, the symmetry breaking did not persist all the way to the surface.

Several other experiments similar to the one described have been carried out to investigate symmetry breaking in cylindrical flows. But none of them seem to have much to do with the phenomenon we have observed.

#### 4.2.2 Similar symmetry breaking in other systems

Phenomena similar to the one we have investigated has been observed in a number of other experiments not directly related to the rotating disk in a cylindrical container.

One example is thermally driven motion in a rotating annulus. Here the setup is comprised of two concentric cylinders with fluid in between. The inner and outer cylinder rotates with the same angular velocity  $\Omega$ , and were it not for the fact that the inner cylinder is cooled and the outer cylinder is heated, the fluid would be in solid body rotation with the cylinders. A weak differential rotation is observed at sufficiently small  $\Omega$  but as  $\Omega$  is increased beyond some critical value, the flow hits an intrinsic instability of the system, and a number of non-axis symmetric waves occur as seen in figure 4.3(a). As  $\Omega$  increases the amplitude, wavenumber and shape of the flow oscillates in a periodic manner or becomes steady, but at even higher  $\Omega$



(a) Streamlines in the rotating annulus. The rotational frequency increases from left to right. Picture taken from (Acheson, 1990) p. 335

(b) Velocity profiles at the exhaust of a turbine engine. Lines (full and dashed) show lines of equal velocity. Picture taken from (Cohen and Wygnanski, 1986)

Figure 4.3: Other systems with properties similar to the rotating disk.

the variations become highly irregular, or chaotic (Acheson, 1990) p.334-335.

Another example is the formation of non-axis symmetric velocity patterns in the exhaust from aircraft turbine engines (Cohen and Wygnanski, 1986). The analogue to our experiment in this case comes from the fact that the rear part of the jet engine consists of a series of rotating plates filled with holes placed in a cylindrical container.

### 4.3 Future work

Although we have covered the basic properties of the system, there are several things to investigate further:

*Theory:* Little or no theory is available in the literature to explain the phenomena we observe. Therefore, developing such a theory would be one of the main goals of any further investigation.

*Phase locking:* Although we did examine how the frequency of the shapes was related to that of the plate, we would have done it more thoroughly if we had the time. The phase locking was done in the 194mm setup, mostly because it was much easier to measure the frequency of especially the 4 corner shapes there, but it would be interesting to examine the phase locking in the old 131mm setup, because we would be able to measure the frequency locking parameters for the  $k=5,6$  states.

*Periodically varying states  $0_a \rightarrow 0_b \rightarrow 2_b \rightarrow 0_a \rightarrow \dots$ :* It would be interesting to measure the period of a periodically varying state and incorporate them in the phase diagram. It would also be interesting to check if they are stable and can oscillate for, say a couple of hours, or if the system eventually relaxes to one of the states in the cycle.

*Surface profile:* It could be interesting to look into the profile of the free surface as seen from the side because it possibly contains a great deal of information about the internal flow of the system. Also, to find the slope of the fluid in the corners of the shapes would be interesting. During our observations we observed that the slope of the fluid in the corners of some of the shapes was almost infinite or even negative.

## 4.4 Concluding remarks

Throughout this report we have described the surprising phenomenon of symmetry breaking in the free surface of water. We have described all the visual properties of the system by presenting some of the hundreds of pictures and movie recordings made over the course of this project.

We have made measurements of the different states of the system and have presented them in various ways. Altogether we have gathered more than 1200 single data points, all of which have been collected manually.

We have presented results that describe important physical properties of the system, most notably by drawing the surprising conclusion that the phenomenon at play is not viscous, and by presenting the phase diagram.

Though we have not been able to find an answer for all the questions that have arisen in the process of making this project, we have gained much knowledge about the system and the next step will be to start searching for a theoretical model to describe the phenomenon.

# Notation

| Name       | Unit         | Meaning  | Size   |
|------------|--------------|--|--|
| $R$        | mm           | Radius of the cylinder                                 |  |
| $H$        | mm           | Water level above the rotating plate at $\Omega_p = 0$ |  |
| $\Omega_p$ | rad/s        | The rotational frequency of the bottom plate           |  |
| $f$        | 1/s=[Hz]     | Same as above, but used in figures.                    |  |
| $\Omega_c$ |              | Number read off the frequency generator                |  |
| $\Omega_w$ | rad/s        | Rotational frequency of the water                      |  |
| $\Omega_k$ | rad/s        | Rotational frequency of a $k$ -corner shape            |  |
| $k$        | -            | Number of corners in a particular shape                |  |
| $\nu$      | $m^2 s^{-1}$ | Kinematic viscosity of water                           | $8.64 \cdot 10^{-7} m^2 s^{-1}$                  |
| $\nu_e$    | $m^2 s^{-1}$ | Kinematic viscosity of ethylene glycol                 | $17.8 \cdot \nu = 1.54 \cdot 10^{-5} m^2 s^{-1}$ |

# Bibliography

- D. J. Acheson. *Elementary Fluid Dynamics*. Oxford University Press, 1990.
- J. Cohen and I. Wygnanski. The evolution of instabilities in the axisymmetric jet. part 2. the flow resulting from the interaction between two wave. *J. Fluid Mech.*, 176:221–235, 1986.
- Ph. D. D. R. Lide. *CRC Handbook of Chemistry and Physics*. CRC Press, Inc., 76 edition, 1995.
- A. H. Hirsá, J. M. Lopez, and R. Miraghaie. Symmetry breaking to a rotating wave in a lid-driven cylinder with a free surface: Experimental observation. *Physics of fluids*, 14, number 6, 2002.
- T. Von Kármán. Über laminare und turbulente reibung. *ZAMM*, 1:233–252, 1921.
- B. Lautrup. *Physics of Continuos Matter*. NBI press, 2002. Yet to be published, draft 7.4.
- J. M. Lopez, F. Marques, A. H. Hirsá, and R. Miraghaie. Symmetry breaking in free-surface cylinder flows. *J. Fluid Mech.*, 502:99–126, 2003.
- M. Mory and A. Spohn. Vortex flow generated by a rotating disk. In E. J. Hopfinger, editor, *Rotating Fluids in Geophysical and Industrial Applications*, chapter V.4. Springer-Verlag, 1992.
- H. Schlichting. In K. Gersten, editor, *Boundary Layer Theory*. Springer, 8 edition, 1999.
- A. Spohn, M. Mory, and E. J. Hopfinger. Observation of vortex breakdown in an open cylindrical container with a rotating bottom. *Experiments in Fluids*, 14: 70–77, 1993.
- M. C. Thompson and K. Hourigan. The sensitivity of steady vortex breakdown bubbles in confined cylinder flows to rotating lid misalignment. *J. Fluid Mech.*, 496:129–138, 2003.

# Appendix

## A.1 The von Kármán model

Von Kármán (Kármán, 1921) considered the flow above a rotating disk of infinite radius with the fluid of density  $\rho$  and viscosity  $\nu$  at rest far from the disk. Consider the cylindrical coordinate system,  $r, \theta, z$ , illustrated in figure A.1. The rotating disk is placed at  $z = 0$ , and rotates with constant angular velocity  $\omega_0$  about the axis  $r = 0$ . If we let  $u, v$  and  $w$  be the velocity in the  $r, \theta$  and  $z$  direction, the flow is determined by the Navier-Stokes equations in cylindrical coordinates

$$uu_r + wu_z - \frac{v^2}{r} = -\frac{1}{\rho}p_r + \nu \left( u_{rr} + \frac{1}{r}u_r + u_{zz} - \frac{u}{r^2} \right), \quad (\text{A.6})$$

$$wv_r + wv_z - \frac{uv}{r} = \nu \left( v_{rr} + \frac{1}{r}v_r + v_{zz} - \frac{v}{r^2} \right), \quad (\text{A.7})$$

$$uw_r + ww_z = -\frac{1}{\rho}p_z + \nu \left( w_{rr} + \frac{1}{r}w_r + w_{zz} \right), \quad (\text{A.8})$$

and the continuity equation

$$\frac{1}{r}(ru)_r + w_z = 0, \quad (\text{A.9})$$

where e.g.  $v_r$  denotes differentiation with respect to  $r$ .

The boundary conditions are

$$\begin{aligned} u = w = 0 \quad \text{and} \quad v = \omega_0 r \quad \text{for} \quad z = 0, \\ u = w = 0 \quad \text{for} \quad z \rightarrow \infty. \end{aligned}$$

To solve the equations A.6-A.9, we use the trial solutions

$$\begin{aligned} u &= r\omega_0 F(Z), \\ v &= r\omega_0 G(Z), \\ w &= \sqrt{\nu\omega_0} H(Z), \\ p &= p_0 + \rho\nu\omega_0 P(Z), \end{aligned}$$

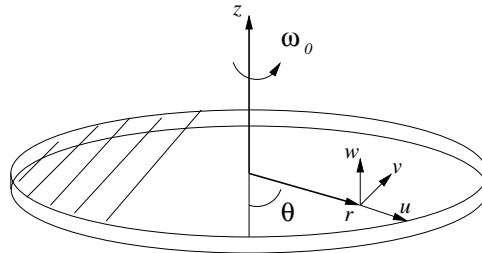


Figure A.1: *The rotating disk.*

where the variable  $Z$  is defined as  $Z = \sqrt{\frac{\omega_0}{\nu}}z$ . Inserting these functions in A.6-A.9 we get a set of ordinary differential equations depending only on the single variable  $Z$

$$F^2 - G^2 + HF' - F'' = 0, \quad (\text{A.10})$$

$$2GF + HG' - G'' = 0, \quad (\text{A.11})$$

$$2F + H' = 0, \quad (\text{A.12})$$

$$P' + HH' - H'' = 0, \quad (\text{A.13})$$

with the boundary conditions

$$F(0) = H(0) = P(0) = 0,$$

$$G(0) = 1,$$

$$F(\infty) = G(\infty) = 0.$$

The solutions of A.10-A.12 was carried out by von Kármán in (Kármán, 1921).

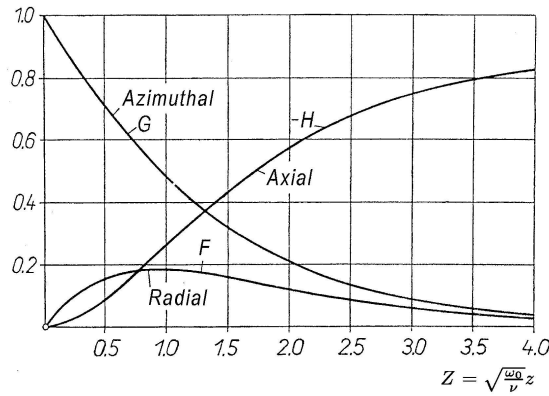


Figure A.2: *Dimensionless velocity profiles.*

Figure 1.5 shows the streamlines, and figure A.2 shows the dimensionless velocity components. The viscous forces drags the fluid near the disk radially outwards under the action of the centrifugal force. The displaced fluid is replaced by some new fluid which is axially sucked into the boundary layer i.e. the rotating disk is in fact acting as a centrifugal pump. (Mory and Spohn, 1992, Schlichting, 1999)